Comparative Analysis of Satellite Relative Dynamics and Fuel-Optimal Trajectory Planning of Satellites Using Minimum Distance Assignment

Himadri Basu, Yasaman Pedari, Mads Almassalkhi, Hamid R. Ossareh

***Abstract*— In this paper, we present a fuel-optimal trajectory optimization (TO) problem for satellite formation flying (SFF) in near-circular low-earth orbits (LEO) under perturbations and modeling uncertainties. Non-spherical gravity (J2) of the earth and air drag are two dominant perturbing forces in LEO which cause significant orbital measurement errors and eventually sub-optimal actuation and trajectory prediction by the TO algorithm. By quantifying uncertainties and modeling errors associated with various relative dynamical models of satellites, we identify a model that is suitable for the TO problem. However, one of the key challenges to design of a computationally efficient TO algorithm for satellite swarms pertains to the assignment of each satellite to a location in a given final formation. To address this, we first decouple the final configuration assignment problem from the TO, derive minimum distance assignment between initial and final formation pairs, and then by using this minimum distance assignment in the TO algorithm, we efficiently compute near-optimal trajectories and actuation under given mission specifications. Our proposed formulation is scalable to large swarm sizes and it allows the computation load to be distributed over the satellite swarm at the expense of small loss in fuel-optimality.**

I. Introduction

Formation flying of LEO spacecrafts has received significant research attention in recent years because of several potential applications in performing complex missions, such as distributed imaging of earth's surface, atmospheric sampling, and interferometry at reduced costs, increased flexibility, reconfigurability and performance compared to a monolithic spacecraft [1]. The primary goal of satellite formation flying (SFF) [2] is to place a cluster of cooperative satellites into nearby orbits to achieve a group objective.

SFF missions typically require complex reconfiguration maneuvers such as moving, reorienting, and rotating a fleet of spacecrafts from an initial configuration to a desired target configuration. It is important to carry out these maneuvers in a fuel-optimal manner while satisfying physical and mission-specific constraints. Fuel/time-optimal control of spacecraft formation based on linear programming was presented in the works of [3]–[5] and with nonlinear programming in [2]. In general, SFF with small formation size has been well-studied in the literature. Interested readers, please refer to [6], [7] and references therein. However, in [2], [3], [5], relative dynamical model of satellites used in the TO does not take into account the J2 perturbation, which is the most dominant perturbing force [8], [9]. Additionally, the nonconvex optimization constraints in [2] make the TO algorithm computationally hard and inapplicable for large swarms. In contrast to these works, our objective in this paper is to propose a computationally efficient, scalable TO framework which devotes due consideration on modeling accuracy of satellites in LEO, capturing the effects of both the J2 perturbation and air drag with sufficient accuracy.

A high-fidelity nonlinear model considering the effects of J2 drift was developed in [10] for a formation keeping problem, which was later extended to include the effects of air drag in [1]. As the model's complexity hampers its application in control designs [11], we present here a comparative analysis of various dynamical models. By quantifying modeling errors, we identify an appropriate model specific to LEO SFF mission design. Specifically, in this work, we revisit four relative dynamical models - namely: (i) high fidelity nonlinear model in [1] that considers both the effects of J2 and air drag, (ii) linearized J2 model in [10], (iii) Hill's equations (Hill-Clohessy-Wiltshire model or HCW model) in [12], (iv) Modified Hill's equations with J2 in [13]. To select an appropriate model for TO, we first compare relative dynamical models (ii)-(iv), stated above, with respect to the high fidelity nonlinear model (i) and compute modeling errors for various initial conditions. This analysis has not been conducted in a cohesive manner before, and modeling errors have not been formally quantified. We fill this gap and quantify the errors, which allows us to identify the linearized J2 as an excellent candidate to be used as computationally simple state-space constraints in the TO problem.

One of the main challenges in designing a computationally efficient TO algorithm is the assignment of satellites in a fuel-optimal configuration on the final formation. Given a set of final positions and velocities, the objective of this assignment problem is to assign each satellite to a specific final destination in a way that is fuel optimal for the entire fleet. We present here an alternative approach to decouple the final configuration assignment problem from the trajectory planning problem to make this more computationally tractable at the expense of a small loss (at most 10%) in fuel-optimality. To this end, instead of simultaneously finding fuel-optimal final assignment and trajectories, we rather solve separately a "minimum cost transportation problem" to derive the shortest distance assignment between initial and final formation pairs [14]. Then, by using the computed final assignments, we efficiently find alternative near-optimal trajectories and actuation profiles. The assignment problem can be solved efficiently in a centralized manner (e.g., by

The authors are with the Department of Electrical and Biomedical Engineering, University of Vermont, Burlington, VT 05405, USA. Email: himadri.basu@uvm.edu, yasaman.pedari@uvm.edu, malmassa@uvm.edu, hossareh@uvm.edu.

This work was supported by NASA under cooperative agreement VT-80NSSC20M0213.

one of the satellites), while the TO problem can be solved by each satellite in a decentralized fashion.

Contributions: In summary, this work presents a computationally efficient trajectory planning algorithm of SFF, which is appropriate for coordination and control in practical missions involving large swarms. The main contributions are: (1) quantification of uncertainties around different satellite relative dynamic models, and selection of the linearized J2 model as suitable for the TO problem (discussed in Sections III, IV), (2) decoupling of the assignment algorithm from the TO problem to efficiently compute near-optimal satellite trajectories (presented in Section VI). Such decoupled formulation allows the satellites to compute their own trajectory in a decentralized manner and the computation load is thus distributed over the satellite swarm.

II. Problem Statement

Given initial and final formation of N identical satellites in close proximity in near-circular LEO subject to J2 gravity and air drag, the objective of this paper is to derive a computationally efficient, scalable TO framework satisfying all physical and mission specific constraints, discussed below, such that all these satellites under predicted actuation from the trajectory planning algorithm, reach the final formation after a specified time duration with minimal fuel consumption. The results presented here are relevant, for example, to interferometric space missions where a satellite cluster reconfigures its formation to create effective beam angles for capturing images while traversing along a "target orbit". We formally define the term "target orbit" in the upcoming section.

Mission requirements: We now summarize the mission specifications for illustrative numerical simulations presented in this paper. Inspired by a formation flying space mission TechSat-21 [15] by U.S. Air Force Research Laboratory (AFRL) in 2006 and their mission specifications, the position tolerance of the desired relative states in this work are chosen to be 5 m in radial, along-track and across-track directions with respect to the "target orbit". Additionally, in the current SFF mission, we assume that the initial "target orbit" is circular or near-circular and all the satellites are initially located within 15 km from this "target orbit". Each satellite is equipped with three thrusters of 3 mN actuation limits with each pointing respectively in radial, along-track and across-track direction. We assume in this work that the thrusters are aligned perfectly with body axes and that they do not induce any torque on the body. Of course, this may not be a realistic assumption and, in practice, reaction wheels and low-level controllers may be employed to counteract any induced rotation (this is outside the scope of this paper). The robust optimal actuation force, as predicted by the trajectory planner here is applicable to other thruster configurations as well, namely coupling thrusters and reaction wheels/magnetometers through an appropriate control allocation scheme.

III. Review of various relative dynamical models of satellites

In this section, we review various relative dynamical models of LEO satellites, capturing primarily the effects of J2 perturbation and air drag. For brevity, through the rest of the paper, we use shorthand notation for trigonometric identities such as $\mathrm{s}_\theta = \sin\theta, \mathrm{c}_\theta = \cos\theta$.

In the traditional texts on dynamical motion of satellites, a virtual unactuated satellite or a fictitious moving point is usually taken as a reference and all N participating satellites in formation as followers. Given the initial orbital elements, the position and velocity vectors of this reference satellite at every time instant define a "target orbit". This target orbit is generally expressed in Earth-centered inertial (ECI) coordinate frame which has its origin located at the center of the earth, X axis aligned with earth's mean equator and passes through vernal equinox, Z axis along the celestial north pole while the Y axis completing the right hand orthogonal frame with the other two [13]. Considering the two main disturbances, namely J2 and atmospheric drag, the differential equations governing the motion [1] of the target orbit are:

$$\dot{r} = v_x, \tag{1}$$

$$\dot{v}_x = -\frac{\mu}{r^2} + \frac{h^2}{r^3} - \frac{K_{J2}}{r^4}(1 - 3\mathrm{s}_i^2\mathrm{s}_\theta^2) - C\|\mathbf{V}_a\|v_x, \tag{2}$$

$$\dot{h} = -\frac{K_{J2}}{r^3}\mathrm{s}_i^2\mathrm{s}_{2\theta} - C\|\mathbf{V}_a\|(h - \omega_e r^2 \mathrm{c}_i), \tag{3}$$

$$\dot{\Omega} = -\frac{2K_{J2}}{hr^3}\mathrm{c}_i\mathrm{s}_\theta^2 - \frac{C\|\mathbf{V}_a\|\omega_e r^2 \mathrm{s}_{2\theta}}{2h}, \tag{4}$$

$$\dot{i} = -\frac{K_{J2}}{2hr^3}\mathrm{s}_{2i}\mathrm{s}_{2\theta} - \frac{C\|\mathbf{V}_a\|\omega_e r^2 \mathrm{s}_i \mathrm{c}_\theta^2}{h}, \tag{5}$$

$$\dot{\theta} = \frac{h}{r^2} + \frac{2K_{J2}\ \mathrm{c}_i^2\mathrm{s}_\theta^2}{hr^3} + \frac{C\|\mathbf{V}_a\|\omega_e r^2 \mathrm{c}_i \mathrm{s}_{2\theta}}{2h}, \tag{6}$$

where r and v_x are respectively the orbital position and velocity in ECI coordinates, h, Ω, i, θ denote angular momentum, right ascension of the ascending node (RAAN), inclination angle and true anomaly, $C = 0.5 C_d \frac{A}{m}\rho$, C_d is air drag coefficient, A is the cross-section area and m is the mass of the spacecraft, ρ is atmospheric density,

$$\mathbf{V}_a = \begin{bmatrix} v_x & (\frac{h}{r} - \omega_e r \mathrm{c}_i) & \omega_e r \mathrm{c}_\theta \mathrm{s}_i \end{bmatrix}^{\mathrm{T}}$$

is the orbital velocity vector with respect to the atmosphere, $\omega_e = 7.2921 \times 10^{-5}\ \mathrm{rad\,s^{-1}}$, $\mu = 398600\ \mathrm{km\,s^{-2}}$ is gravitational constant, $K_{J2} = 1.5\mu J_2 R_e^2$ with second zonal harmonic constant $J_2 = 1.082 \times 10^{-3}$, and earth's mean equatorial radius $R_e = 6378$ km.

The relative dynamical motion of all follower satellites are described in local-vertical-local-horizontal (LVLH) frame [16], with its origin located on the target orbit. In this local coordinate frame, the relative position vector of j^{th} spacecraft is usually expressed as $\bar{\mathbf{r}}_j = \begin{bmatrix} x_j & y_j & z_j \end{bmatrix}^{\mathrm{T}}$ where the unit vectors associated with x_j, y_j and z_j respectively point in the radial, along-track and across-track directions. Thrust vectors of the follower satellites u_{jx}, u_{jy} and u_{jz} respectively point

in the radial, along-track and across-track directions in LVLH frame. Furthermore, the net perturbation force comprising of J2 effects and air drag is pointed towards the origin of ECI reference frame.

A. High fidelity nonlinear relative dynamical model

As described in [1], the equations of motion for j^{th} spacecraft under J2 perturbation and atmospheric drag, relative to the target orbit are given as follows.

$$\begin{aligned}\ddot{x}_j &= 2\dot{y}_j\omega_z - x_j(n_j^2-\omega_z^2) + y_j\alpha_z - z_j\omega_x\omega_z + a_{jx}\\ &\quad - \bar{\zeta}\mathrm{s}_i\mathrm{s}_\theta - r(n_j^2-n^2) - l_{1j}(\dot{x}_j - y_j\omega_z) - l_{2j}v_x, \qquad (7)\\ \ddot{y}_j &= -2\dot{x}_j\omega_z + 2\dot{z}_j\omega_x - x_j\alpha_z - y_j(n_j^2-\omega_z^2-\omega_x^2)\\ &\quad + z_j\alpha_x - \bar{\zeta}\mathrm{s}_i\mathrm{c}_\theta - l_{1j}(\dot{y}_j + x_j\omega_z - z_j\omega_x) + l_{3j} + a_{jy}, \qquad (8)\\ \ddot{z}_j &= -2\dot{y}_j\omega_x - x_j\omega_x\omega_z - y_j\alpha_x - z_j(n_j^2-\omega_x^2) - \bar{\zeta}\mathrm{c}_i\\ &\quad - l_{1j}(\dot{z}_j + y_j\omega_x) - l_{2j}\omega_e r\mathrm{c}_\theta\mathrm{s}_i + a_{jz}, \qquad (9)\end{aligned}$$

where $l_{1j} = C\|\mathbf{V}_{aj}\|$, $l_{3j} = l_{2j}(\frac{h}{r} - \omega_e r\mathrm{c}_i)$, $l_{2j} = C(\|\mathbf{V}_{aj}\| - \|\mathbf{V}_a\|)$, $\bar{\zeta} = \zeta_j - \zeta$, $\mathbf{V}_{aj}$ is the velocity of the j^{th} spacecraft with respect to the atmosphere, a_{jx}, a_{jy} and a_{jz} are control accelerations respectively in x, y, z directions of the LVLH frame,

$$\zeta = \frac{2K_{J2}\mathrm{s}_i\mathrm{s}_\theta}{r^4}, \zeta_j = \frac{2K_{J2}r_{jZ}}{r^5}, \qquad (10a)$$

$$n^2 = \frac{\mu}{r^3} + \frac{K_{J2}}{r^5} - \frac{5K_{J2}\mathrm{s}_i^2\mathrm{s}_\theta^2}{r^5}, \qquad (10b)$$

$$n_j^2 = \frac{\mu}{r_j^3} + \frac{K_{J2}}{r_j^5} - \frac{5K_{J2}r_{jZ}^2}{r_j^7}, \qquad (10c)$$

$$r_j = \sqrt{(r+x_j)^2 + y_j^2 + z_j^2}, \qquad (10d)$$

$$r_{jZ} = (r+x_j)\mathrm{s}_i\mathrm{s}_\theta + y_j\mathrm{s}_i\mathrm{c}_\theta + z_j\mathrm{c}_i. \qquad (10e)$$

$$\alpha_z = -\frac{2hv_x}{r^3} - \frac{K_{J2}}{r^5}\mathrm{s}_i^2\mathrm{s}_{2\theta}, \qquad (10f)$$

$$\alpha_x = f_x - \frac{K_{J2}\mathrm{s}_{2i}\mathrm{c}_\theta}{r^5} + \frac{3v_xK_{J2}\mathrm{s}_{2i}\mathrm{s}_\theta}{r^4h} - p_x, \qquad (10g)$$

$$f_x = -C\|\mathbf{V}_a\|\omega_e\left(\frac{2rv_x\mathrm{c}_\theta\mathrm{s}_i}{h} - \left(\frac{r}{h}\right)^2\mathrm{c}_\theta\mathrm{s}_i\dot{h} + g_x\right), \qquad (10h)$$

$$g_x = -\frac{r^2\mathrm{s}_\theta\mathrm{s}_i\dot{\theta}}{h} + \frac{r^2\mathrm{c}_\theta\mathrm{c}_i\dot{i}}{h},\ p_x = \frac{8K_{J2}^2\mathrm{s}_i^3\mathrm{c}_i\mathrm{s}_\theta^2\mathrm{c}_\theta}{r^6h^2} \qquad (10i)$$

with $\dot{h}$, $\dot{i}$ and $\dot{\theta}$ being given respectively in (3), (5), (6).

B. Linearized J2 model

In the high fidelity nonlinear model (7) – (10), there are nonlinear terms n_j^2, ζ_j which include polynomials of the reciprocal of r_j and consequently x_j, y_j, z_j. By using Gegenbauer polynomials, the terms n_j^2 and ζ_j were shown to bear a linear relationship in [10] with the decision variables x_j, y_j and z_j as follows

$$\zeta_j = \zeta - \frac{8K_{J2}x_j\mathrm{s}_i\mathrm{s}_\theta}{r^5} + \frac{2K_{J2}y_j\mathrm{s}_i\mathrm{c}_\theta}{r^5} + \frac{2K_{J2}z_j\mathrm{c}_i}{r^5},$$

$$n_j^2 = n^2 - \frac{3\mu x_j}{r^4} - \frac{5K_{J2}}{r^6}\left[x_j(1-5\mathrm{s}_i^2\mathrm{s}_\theta^2) + y_j\mathrm{s}_i^2\mathrm{s}_{2\theta} + z_j\mathrm{s}_{2i}\mathrm{s}_\theta\right].$$

With the above substitution, the first order linear J2 model yields the following time-varying dynamics

$$\begin{aligned}\ddot{x}_j &= \frac{2\dot{y}h}{r^2} + x_j\left(\frac{2\mu}{r^3} + \frac{h^2}{r^4} + \frac{4K_{J2}(1-3\mathrm{s}_i^2\mathrm{s}_\theta^2)}{r^5}\right) + a_{jx}\\ &\quad - y_j\left(\frac{2v_xh}{r^3} - \frac{3K_{J2}\mathrm{s}_i^2\mathrm{s}_{2\theta}}{r^5}\right) + \frac{5K_{J2}\mathrm{s}_{2i}\mathrm{s}_\theta}{r^5}, \qquad (11)\\ \ddot{y}_j &= -\frac{2\dot{x}_jh}{r^2} - \frac{2K_{J2}\dot{z}_j\mathrm{s}_{2i}\mathrm{s}_\theta}{r^3h} + x_j\left(\frac{2v_xh}{r^3} + \frac{5K_{J2}\mathrm{s}_i^2\mathrm{s}_{2\theta}}{r^5}\right)\\ &\quad - y_j\left(\frac{\mu}{r^3} - \frac{h^2}{r^4} + \frac{K_{J2}(1+2\mathrm{s}_i^2-7\mathrm{s}_i^2\mathrm{s}_\theta^2)}{r^5}\right)\\ &\quad + z_j\left(\frac{3K_{J2}v_x\mathrm{s}_{2i}\mathrm{s}_\theta}{r^4h} - \frac{2K_{J2}\mathrm{s}_{2i}\mathrm{c}_\theta}{r^5}\right) + a_{jy}, \qquad (12)\\ \ddot{z}_j &= \frac{2K_{J2}\dot{y}_j\mathrm{s}_{2i}\mathrm{s}_\theta}{r^3h} + \frac{5K_{J2}x_j\mathrm{s}_{2i}\mathrm{s}_\theta}{r^5} - \frac{3K_{J2}y_jv_x\mathrm{s}_{2i}\mathrm{s}_\theta}{r^4h}\\ &\quad - z_j\left(\frac{\mu}{r^3} + \frac{K_{J2}(3-2\mathrm{s}_i^2-5\mathrm{s}_i^2\mathrm{s}_\theta^2)}{r^5}\right) + a_{jz}, \qquad (13)\end{aligned}$$

where r, v_x, h, θ, i are time-varying forcing terms obtained by solving Eqs. (1)–(6).

C. Hill-Clohessy-Wiltshire (HCW) Model with J2

A modified HCW model considering earth's J2 non-spherical effect [13] is given as follows

$$\ddot{x}_j = a_{jx} + 2nc\dot{y}_j + (5k_1^2 - 2)n^2x_j, \qquad (14)$$

$$\ddot{y}_j = a_{jy} - 2nc\dot{x}_j, \qquad (15)$$

$$\ddot{z}_j = a_{jz} - k_2^2z_j, \qquad (16)$$

where $k_2 = nk_1 + 1.5J_2\left(\frac{R_e\mathrm{c}_i}{r}\right)^2$, $k_1 = \sqrt{1+k_3}$, $k_3 = 0.375J_2\left(\frac{R_e}{r}\right)^2(1+3\mathrm{c}_{2i})$. In the absence of J2 perturbations, equations (14) – (16) reduce to original HCW model or popularly known as Hill's equation [17].

IV. Uncertainty quantification and modeling errors

In this section, we compare various dynamical models presented above and evaluate the modeling errors for numerous initial conditions. We are also interested to determine the time instant when the modeling errors go beyond a realistic position tolerance of 5 m [3]. For a given initial condition, we consider a model to be accurate till the time it is within this threshold value. This analysis helps us to determine which model should be used in the TO optimization for a given time window and initial relative position of satellites.

For a given initial position and simulation time window, the modeling error of the linearized J2 model is evaluated as the maximum relative distance between the trajectories generated by (11) – (13) and the nonlinear model (7) – (9) over the time window under consideration. Modeling error for HCW with or without J2 are analogously computed with respect to the nonlinear model. For convenience, we denote an orbital period of time with T, where $T = 2\pi\sqrt{\frac{a^3}{\mu}}$.

In Fig. 1, we present the maximum modeling errors of the three linear models relative to the high fidelity nonlinear

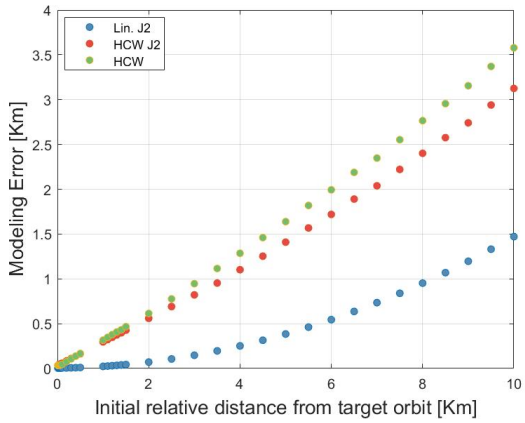

Fig. 1: Maximum modeling error of the three models - Linearized J2, HCW with and without J2 relative to high fidelity nonlinear model (7) – (9) for initial relative distance (LVLH frame) $[0.01, 15]$ km and simulation time length $5T$.

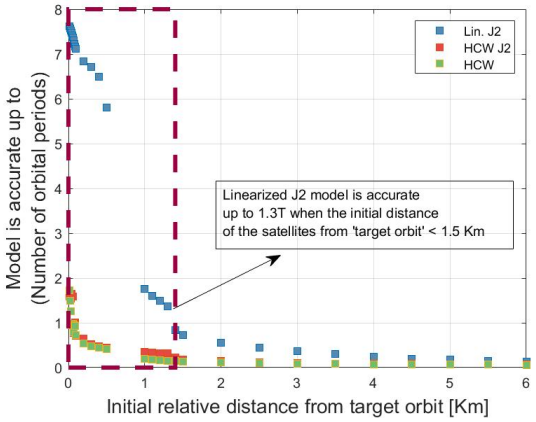

Fig. 2: Accuracy of the three models in terms of the length of time elapsed - linearized J2, HCW with and without J2 for initial relative distance (LVLH frame) $[0.01, 6]$ km. Corresponding to a specific initial distance, the figure shows the duration until which the trajectory error is smaller than 5 m and a model is deemed accurate.

model (7) – (9) under a sinusoidal actuation with frequencies within $[0, 1]$ rad s^{-1}, amplitudes between $[-3, 3]$ mN in a simulation for $5T$ and initial positions drawn randomly from a uniform distribution such that the relative distance for these initial points from the origin lie between $[0.01, 15]$ km. Corresponding to a specific initial distance from the origin in LVLH frame, we randomly pick 150 initial positions, evaluate the maximum of modeling errors for these initial positions and replicate this approach for other initial relative distances and models. From Fig. 1, we observe that the linearized J2 model is more accurate as compared to the other models under considered sinusoidal actuation. We verified this to be true even when there is no actuation.

Next, we evaluate the duration in which all three models yield less than 5 m modeling error under aforementioned sinusoidal actuation. In addition to the modeling errors, we also evaluate the corresponding time instant when this model error exceeds beyond 5 m. The simulation results showing the accuracy of all three models are presented in Fig. 2 from which we observe again that the linearized J2 model is more accurate than the others. Precisely, when the initial distance from the target orbit is within 1.5 km (marked by the rectangular box), linearized J2 model error is within 5 m for more than T duration. Therefore by considering both the modeling error and accuracy time horizon, linearized J2 model is the most appropriate candidate to formulate the relative dynamics of satellite swarms in TO problem with initial distance within 1 km and final time $t_f = T$. For practical mission purposes, where $t_f > T$, we re-optimize the TO periodically after an interval of length T.

V. Formulation of the Basic TO Problem

This section presents a basic TO formulation of satellite swarm, modeled as the mixed-integer linear program (MILP) as in [3], [5]. The core of this optimization problem is to select state variables $p_i(k) = \begin{bmatrix}\bar{p}_i(k) & \dot{\bar{p}}_i(k)\end{bmatrix}^{\mathrm{T}}, \bar{p}_i = \begin{bmatrix}x_i & y_i & z_i\end{bmatrix}^{\mathrm{T}}$, corresponding control $u_i(k)$ for each spacecraft $i = \{1, 2, \cdots, N\}$ satisfying Euler-discretized version of linearized J2 dynamics (11) – (13) in the form

$$\begin{aligned} &p_i(k+1) = A(k)p_i(k) + Bu_i(k), k = 0, 1, \cdots, N_k - 1 \\ &p_i(0) = p_{iS}, p_i(N_k) = p_{iT}, \end{aligned} \tag{17}$$

where p_{iS} and p_{iT} are respectively the initial and terminal state vectors for i^{th} spacecraft, and N_k is the terminal time step. Similar to [3], [5], we consider that inputs thrust vectors along with their respective slew rates lie within a specified bound

$$-u_{m,max} \leq u_{im}(k) \leq u_{m,max}, \ m = 1, 2, 3, \tag{18}$$

$$u^r_{m,min} \leq u_{im}(k+1) - u_{im}(k) \leq u^r_{m,max}, \tag{19}$$

where $u_{im}(k)$ denotes the m^{th} component of $u_i(k)$ with its rate limit being bounded within $\left[u^r_{m,min}, u^r_{m,max}\right]$.

In contrast to traditional TO problems with well known final configuration [2], we consider that the assignment of the final configuration to each satellite is not known *a priori*. Assignment of final configuration, also known as path assignment (PA) problem, is formulated with mixed-integer linear constraints, given as follows

$$p_{iT} = \sum_{j=1}^{N} b_{ij} p_{jD}, \sum_{i=1}^{N} b_{ij} = 1, \sum_{j=1}^{N} b_{ij} = 1, \tag{20}$$

where $p_{jD}, \ j = 1, 2, \cdots, N$ denotes all destination locations available for a satellite to occupy, the unity row sum and column sum of the assignment matrix $\mathcal{B} = [b_{ij}]_{N \times N}$ ensures that each of these terminal points $p_{iD}, \ i = 1, 2, \cdots, N$ is assigned to only one of the satellites. The objective of this TO problem with final configuration constraints, referred to as coupled PATO problem is to minimize the total fuel consumption by all N satellites over the entire time horizon

$$\min_{u,p,\mathcal{B}} J = \sum_{i=1}^{N} \sum_{k=0}^{N_k - 1} \sum_{m=1}^{3} |u_{im}(k)|$$

subject to (17) – (20). However, solving this TO for a formation reconfiguration problem with just three satellites in a standard Windows computer (3.8 GHz CPU, 16 GB memory) takes nearly 8 minutes to compute optimal trajectories and control using a mixed-integer solver such as Gurobi [18]. Due to the inclusion of N^2 binary variables associated with the final assignment constraint (20) within the TO problem, the resulting computational complexity is prohibitive. To improve the computationally efficiency with the current processing capabilities, we thus present in Section VI alternative approaches to reformulate TO.

VI. Main Results

To make the trajectory planning framework, formulated as coupled PATO problem in Section V computationally efficient and scalable, our proposed approach decouples the assignment problem from TO and the resulting formulation is referred to as decoupled PATO problem throughout the text. The high-level idea is that, by solving a "transportation problem" [14], we derive a final configuration of satellites which are at the minimum overall distance from the initial formation assignment.

A. MILP formulation of the decoupled PATO problem

The final configuration of satellites based on minimum distance assignment is formulated as

$$\text{Decoupled PA problem: } \min_{\mathcal{B}} J_D = \sum_{i=1}^{N}\sum_{j=1}^{N} d_{ij} b_{ij}$$

subject to $\sum_{i=1}^{N} b_{ij} = 1, \sum_{j=1}^{N} b_{ij} = 1$, where $d_{ij} = \|\bar{p}_{jD} - \bar{p}_{iS}\|_2$ denotes the distance between the i^{th} position (corresponds to i^{th} satellite) of the initial formation and j^{th} of the final formation based on Euclidean 2 norm, and b_{ij} is the $(i,j)^{\text{th}}$ element of the binary assignment matrix $\mathcal{B}$. This assignment algorithm, formulated as MILP, is equivalent to well-known "transportation problem" where the objective is to find the path between a pair of initial and final points with minimum cost of transportation. The solution to this optimization problem is the assignment matrix $\mathcal{B}$ that determines the final positions of N satellites. The assignment problem is thus solved in a centralized manner and it scales quadratically with increasing swarm size, as shown in Fig. 3. Moreover, this PA problem has a small solve time, less than 2.5 s for a swarm size of order 500 on a standard laptop computer, and thus minimum distance PA problem is both scalable and computationally efficient.

Given the final configuration of satellites $\bar{p}_{iD}$, $i = 1, 2, \cdots, N$, the structure of the decoupled fuel optimal TO problem is the same as the coupled counterpart in Section V, except for the objective function and final configuration constraint which no-longer have b_{ij} as one of the decision variables. Since, all the satellites now know their respective terminal states p_{iT}, each of them can solve the TO problem in a decentralized manner, using their local computer. Therefore, the objective function of the decoupled TO problem

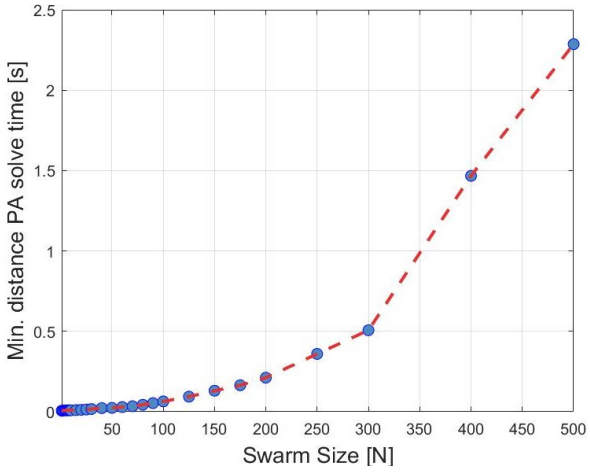

Fig. 3: Computational complexity of the minimum distance PA problem with increasing swarm size

becomes

$$\min_{u,p} \mathbf{J} = \sum_{k=0}^{N_k-1}\sum_{m=1}^{3} |u_{im}(k)|$$

with the terminal state constraint $p_{iT} = \sum_{j=1}^{N} b_{ij} p_{jD}$, where b_{ij} is the solution to the PA problem. We also note here that the final position constraint can also be relaxed and put into the objective function with a large penalty to ensure feasibility of the decoupled TO problem, but we will not pursue that in this paper.

B. Computational Efficiency of Decoupled PATO Formulation

As we have decoupled the assignment problem, the resulting TO algorithm can now be solved by each satellite in a decentralized manner. The computation time is evaluated as the maximum TO solve time of a satellite in the swarm. With discretization time-step of 20 s, solving this decoupled TO problem in a standard Windows computer with a Gurobi solver for a single spacecraft typically takes 0.18 s. Such decoupled PATO formulation is at least 500 times more computationally efficient compared to its coupled counterpart, even for a small formation containing only tens of spacecraft. The proposed decoupled PATO formulation is therefore scalable to large swarm sizes and is computationally efficient.

C. Illustrative Example

Let us now consider a numerical example to illustrate the effectiveness of the decoupled PATO problem as opposed to its coupled counterpart in Section V. Four satellites start from a projected circular orbit (PCO) of 1 km radius around the origin in an LVLH frame and end up being on another PCO of 5 km radius after one orbital period using minimal fuel with available thrust limit being 3 mN. We solve the fuel optimal trajectory planning problem using coupled PATO algorithm based on minimum fuel assignment in Section V, and also with decoupled PATO in VI-A which is based on minimum distance assignment, and consequently evaluate the predicted trajectory errors. Optimal satellite trajectories

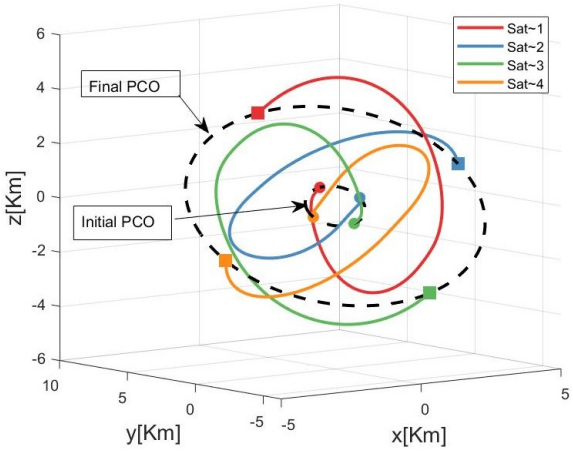

(a) Optimal satellite trajectories under decoupled PATO formulation

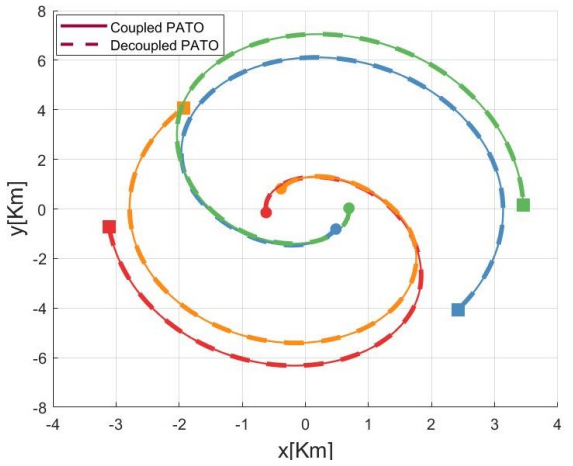

(b) Coupled and decoupled PATO trajectories projected onto x-y plane in LVLH frame

Fig. 4: Optimal satellite trajectories under coupled and decoupled PATO formulation

under decoupled PATO formulation is shown in Figure 4a with initial locations marked in circles and the terminal locations in squares. In Figure 4b, the coupled and decoupled PATO trajectories are projected onto x-y plane and we observe that both formulations yield an identical solution.

D. Relative Loss of Fuel-Optimality of Decoupled PATO Formulation

We now investigate whether the resulting satellite assignments from both approaches are always identical and, if not, compute the loss of optimality as we move from the coupled PATO algorithm based on minimum fuel assignment to decoupled PATO based on the minimum distance assignment. Since the satellite dynamics have six coupled degrees of freedom and are governed by time-varying differential equations, it is not an easy task to analytically find a feasible space of initial and final points for which both the assignments are same. Therefore, with the help of extensive Monte-Carlo simulations, we numerically estimate a probability distribution for identical assignment events and determine the relative fuel cost error between the coupled and decoupled

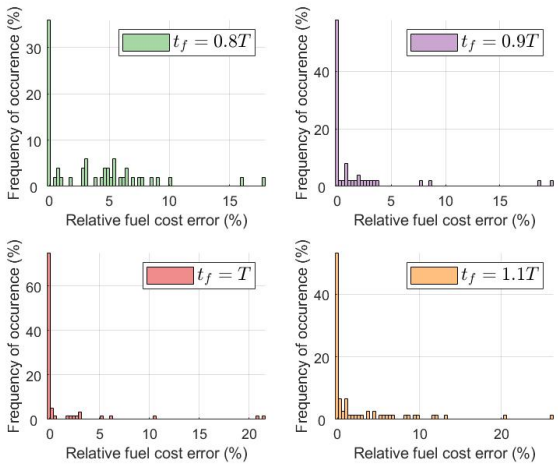

Fig. 5: Probability distribution of relative fuel cost error between coupled and decoupled TO problem for different $t_f \in [0.8T, 1.1T]$ with mean $\mu = 3.5249,\ 1.6992,\ 1.3399,\ 2.45$ and standard deviation $\sigma = 4.08,\ 4.05,\ 4.14,\ 4.83$.

PATO problems when two assignments are different.

For these numerical simulations, we select initial and final positions from two uniform random distributions $\mathcal{U}(-1, 1)$ km, $\mathcal{U}(-5, 5)$ km respectively. Given the actuator saturation of 3 mN, we select the final times t_f from the set $[0.8T, 1.1T]$ to arrive at a feasible solution to the TO problem satisfying all control constraints. If t_f is selected too small, for example $0.3T$ then to reach the destination in such a short period requires a large thrust which may be bigger than 3 mN.

For different final times t_f, the relative fuel cost error between the coupled and decoupled PATO problem and the associated probability distributions are given in Figure 5. For $t_f = 0.8T,\ 0.9T,\ T,\ 1.1T$, there are respectively 36%, 54.55%, 80% and 53.33% cases where minimum distance assignment is same as the minimum fuel assignment. Clearly, as t_f tends to T, we numerically find that the solution to the decoupled PATO problem is identical with its coupled counterpart for about 80% of cases. On either side of $t_f = T$, frequency of such occurrences decrease gradually. Nevertheless, for different final times t_f, there are about 96% cases for which the decoupled fuel cost is at most 10% greater than the coupled PATO cost. Therefore, decoupled PATO algorithm offers a near fuel-optimal, computationally efficient and scalable solution to the trajectory planning problem. However, there are nearly 4% cases in which the decoupled PATO cost is 20% greater than the coupled cost. To address this, one of our future works would be to include the curvature constraints in the decoupled PATO problem.

Remark 1: In this work, we have implicitly assumed that the initial position and velocities of satellites are known precisely. In the presence of uncertainties associated with p_{iS}, the TO algorithm in the previous section, which was based on nominal initial positions, may in this case yield large trajectory prediction errors. Therefore, when x_{iS} is uncertain, a shrinking horizon optimal control is envisioned

as a solution to address this issue and minimize the trajectory prediction errors. Specifically, to avoid accumulation of large modeling errors, we restart the TO algorithm after a small time interval (e.g., every 15 minutes) with new initial points that come from the high fidelity model (7) - (9) or real measurements, a representative of the actual fleet dynamics. This method of successive prediction and re-optimizing the TO with more accurate initial positions yields a more robust control profile that eventually renders a small trajectory prediction error in the face of uncertain initial positions. This shrinking horizon optimal control not only robustifies the TO against initial uncertainties and modeling errors, but also improves fuel-optimality with repeated optimization. Full investigation of this idea is an ongoing research topic.

VII. Conclusions

In this paper, we studied TO problem for SFF mission on circular or near-circular LEO under perturbations and modeling uncertainties. We reviewed several relative dynamical models of the satellites and, for various initial conditions and bounded actuation, we evaluated the modeling errors which eventually allowed us to select the linearized J2 model as the most appropriate candidate for the TO algorithm when the satellite swarm is located within 1.5 km initial distance from the target orbit and trajectory prediction horizon is bounded within 1.3 orbital periods.

Numerical simulations illustrate that the computational challenge of the TO algorithm is exacerbated by the presence of underlying PA problem of the satellites. In this work, we proposed an alternative formulation by (1) decoupling the PA problem from the original trajectory planning algorithm, (2) finding a minimum distance assignment between initial and final formation pairs, (3) solving decentralized TO problem in parallel for all satellites in the swarm. This formulation allows the computation load to be distributed across the swarm, which makes this approach ideal for a large-scale SFF mission. With the help of numerical simulations, we illustrate that such computational advantage of decoupled PATO formulation comes at the expense of 10% loss in fuel-optimality compared to the coupled problem.

Our proposed future work includes introducing curvature constraints in the decoupled TO problem to further improve fuel optimality, studying the shrinking horizon optimal control approach discussed in Remark 1, and considering collision avoidance constraints to maintain a safe inter-satellite distance throughout the maneuver.

Acknowledgement

The authors would like to thank Dr. Ryan McDevitt from Benchmark Space Systems and Dr. Amir Rahmani from NASA's Jet Propulsion Laboratory (JPL) for insightful discussions.

References

[1] D. Morgan, S.-J. Chung, L. Blackmore, B. Acikmese, D. Bayard, and F. Y. Hadaegh, "Swarm-keeping strategies for spacecraft under j2 and atmospheric drag perturbations," *Journal of Guidance Control and Dynamics*, vol. 35, no. 5, pp. 1492–1506, 2012.

[2] H. C. Lim and H. Bang, "Trajectory planning of satellite formation flying using nonlinear programming and collocation," *J. Astron. Space Sci.*, vol. 25, no. 4, pp. 361–374, 2008.

[3] M. Tillerson, G. Inalhan, and J. P. How, "Co-ordination and control of distributed spacecraft systems using convex optimization techniques," *Int. J. Robust Nonlinear Control*, vol. 12, pp. 207–242, 2002.

[4] I. Garcia and J. P. How, "Trajectory optimization for satellite reconfiguration maneuvers with position and attitude constraints," in *Proceedings of the 2005, American Control Conference, 2005.*, vol. 2, Portland, USA, 2005, pp. 889–894.

[5] A. Richards, T. Schouwenaars, J. P. How, and E. Feron, "Spacecraft trajectory planning with avoidance constraints using mixed-integer linear programming," *Journal of Guidance, Control, and Dynamics*, vol. 25, no. 4, pp. 755–764, 2002.

[6] R. Kristiansen and P. J. Nicklasson, "Spacecraft formation flying: A review and new results on state feedback control," *ACTA Astronautica*, vol. 65, pp. 1537–1552, 2009.

[7] D. P. Scharf, F. Y. Hadaegh, and S. R. Ploen, "A survey of spacecraft formation flying guidance and control (part i): Guidance," in *in Proc. of the American Control Conference*, Denver, Colorado, USA, 2003, pp. 1733–1739.

[8] C. W. T. Roscoe, J. D. Griesbach, J. J. Westphal, D. R. Hawes, and J. J. P. Carrico, "Force modeling and state propagation for navigation and maneuver planning for cubesat rendezvous, proximity operations, and docking," *Advances in the Astronautical Sciences*, vol. 150, pp. 573–590, 2014.

[9] M. Eshagh and M. N. Alamdari, "Perturbations in orbital elements of a low earth orbiting satellite," *Journal of the Earth & Space Physics.*, vol. 33, no. 1, pp. 1–12, 2007.

[10] D. Wang, B. L. Wu, and E. K. Poh, *Satellite Formation Flying*, ser. Intelligent Systems, Control and Automation: Science and Engineering. Singapore: Springer, 2017, vol. 87.

[11] G. Xu and D. Wang, "Nonlinear dynamic equations of satellite relative motion around an oblate earth," *Journal of Guidance, Control and Dynamics*, vol. 31, no. 5, pp. 1521–1524, 2008.

[12] G. Inalhan and J. How, "Relative dynamics and control of spacecraft formations in eccentric orbits," *Journal of Guidance, Control, and Dynamics*, vol. 25, no. 1, pp. 48–59, 2002.

[13] J. Ma, "Formation flying of spacecrafts for monitoring and inspection," Master's thesis, Lulea University of Technology, Sweden, 2009.

[14] A. Chaudhuri and K. De, "A comparative study of transportation problem under probabilistic and fuzzy uncertainties," *CoRR*, vol. abs/1307.1891, 2013. [Online]. Available: http://arxiv.org/abs/1307.1891

[15] A. F. R. L. S. V. Directorate, "Techsat 21 factsheet page," https://www.vs.afrl.af.mil/factsheets/TechSat21.html, 2019, online; accessed 8 September 2021.

[16] B. Wu, G. Xu, and X. Cao, "Relative dynamics and control for satellite formation: Accommodating j2 perturbation," *Journal of Aerospace Engineering*, vol. 29, no. 4, p. 04016011, 2016.

[17] M. Sidi, *Spacecraft Dynamics & Control: A Practical Engineering Approach*, ser. Cambridge Aerospace Series. Cambridge University Press, 2006, vol. 7.

[18] Gurobi Optimization, LLC, "Gurobi Optimizer Reference Manual," 2021. [Online]. Available: https://www.gurobi.com